Electrical Power and Energy Systems 141 (2022) 108172

Contents lists available at ScienceDirect

International Journal of Electrical Power and Energy Systems

journal homepage: www.elsevier.com/locate/ijepes

A novel protection scheme to detect, discriminate, and locate electric faults in photovoltaic arrays using a minimal number of measurements

Hossein Bagherzadeh [a], Moein Abedini [a], Mahdi Davarpanah [a], Sadegh Azizi [b,*]

[a] School of Electrical and Computer Engineering, College of Engineering, University of Tehran, Tehran 1439957131, Iran
[b] School of Electronic and Electrical Engineering, University of Leeds, Leeds LS2 9JT, UK

ARTICLE INFO

Keywords:
Electric faults
Ground fault
Line-to-line fault
Open-circuit fault
Photovoltaic arrays protection

ABSTRACT

Quality degradation, power loss, and fire hazards are amongst the consequences of uncleared electric faults within photovoltaic (PV) arrays. This paper proposes an effective protection method for i) detecting electric faults using current variations, ii) discriminating them from other disturbances based on the transient response of PV cells, and iii) locating the faulty string within PV arrays with a minimal number of measurement sensors. To accomplish these, both dynamic and static models of PV cells are taken into account whilst formulating the problem. To evaluate the performance of the proposed method, a prototype solar power plant is simulated under a wide variety of normal and abnormal conditions in PSCAD-EMTDC software. The simulation results verify the proposed method's high speed and desirable accuracy. Independency from meteorological data and the need for a minimal number of measurement sensors are the salient advantages of the proposed method. Therefore, the implementation of this method would be affordable for PV systems of different scales.

1. Introduction

Solar power plants are subject to various failures such as ground fault, line-to-line fault, and open-circuit fault in Photovoltaic (PV) arrays. Electric faults may happen for different reasons, such as cable insulation failure, mechanical damage, and accidental short circuit inside the PV combiner box. If these faults are not detected and cleared in time, the efficiency of the power plant decreases considerably; let alone the possibility of destructive damages to solar modules and fire hazards [1–4].

Traditionally, methods for fault detection in photovoltaic arrays have been mostly based on over-current protection schemes. However, the fault current may not be sufficiently large due to the current-limiting nature of PV cells, non-linearity of the current–voltage (*I-V*) curve, fault resistance, and low solar irradiance. Under these conditions, the over-current-based protection schemes might not provide enough sensitivity for detecting and clearing faults. Another challenge for conventional protection systems is fault location, which is key to reducing the troubleshooting time in large solar farms [4]. Recent research in this context is focused on overcoming the shortcomings of conventional protection schemes and can be classified into three categories:

- **Quantitative model-based methods**: This category includes methods that are based upon the analytical model of the PV system. Authors in [5] suggest a method for fault detection and classification in the PV systems using the variations of the (*I–V*) curve. In [6], the instantaneous current decrease between two MPPT sampling moments is used to identify disturbances and diagnose faults. The protection scheme in [7] is designed based on the magnitude and waveform features of the voltage signal. In [8], a novel approach is introduced that is based on the rate of change of voltage and current during the fault transient phase. Residual current detection (RCD) is utilized to detect the ground faults in the PV array or each string by monitoring the input and output currents [4]. Besides, the comparison of the output power and actual system losses with obtained results from simulations is adopted in [9]. The advantages of these methods are their simple concepts, physical interpretability, and low cost of implementation. Nevertheless, quantitative model-based methods lack advanced features such as fault location capability, are susceptible to simulation model errors, and require a large number of measurement sensors.
- **Signal processing-based methods**: These methods are characterized by their reliance on signal analysis in the time and frequency domain. The discrete wavelet transform [10,11] and Fourier

* Corresponding author.
E-mail addresses: h.bagherzadeh@ut.ac.ir (H. Bagherzadeh), m.abedini@ut.ac.ir (M. Abedini), m.davarpanah@ut.ac.ir (M. Davarpanah), s.azizi@leeds.ac.uk (S. Azizi).

https://doi.org/10.1016/j.ijepes.2022.108172
Received 26 December 2021; Received in revised form 19 March 2022; Accepted 27 March 2022
Available online 6 April 2022

Nomenclature

I_{ph}	Photocurrent caused by the photovoltaic effect.
I_d, I_{sh}	Diode and shunt resistor currents.
I_{scn}	Nominal short-circuit current of the PV cell at STC.
G	Solar radiation intensity.
G_{ref}	Reference irradiation at STC.
α_T	Photocurrent temperature coefficient.
T	PV cell's temperature.
T_{ref}	Reference temperature at STC.
R_s, R_{sh}	Parasitic series and shunt resistors.
V	Terminal voltage of the PV cell.
I_0	Dark diode saturation current.
n, K_B	Diode ideality factor and Boltzmann constant.
q	Electron charge.
R_d	Diode's dynamic resistance.
C_D, C_T	diffusion and transition capacitances.

transform [12] can be adopted for detecting failures, especially faults associated with DC arcs. Time-domain reflectometry (TDR) proves effective to this end, as investigated in [13]. In this approach, the injected signal into the PV system is compared to the reflected signal. Delay and variation of waveforms are analyzed to determine the type and location of the fault [14]. Despite the advantages offered by methods in this category, such as independence of meteorological data, they normally require the PV system to be isolated from the grid and the fault diagnosis process to be executed in offline mode. In addition, their performance can be affected by the noise of the inverter's switching components. They also demand additional equipment, which comes at a high cost.

- **Data driven-based methods:** Methods of this category are reliant on discovering patterns and correlations within large data. For instance, [15] adopts descriptive and inferential statistics to discover faults. In [16], statistical outlier detection rules are suggested to identify the normal and faulty operation of the photovoltaic arrays based on individual string current measurements. The statistical methods do not require weather data or model training. However, they cannot classify the fault type and may become ineffective at low fault mismatch levels. In recent years machine learning techniques have proven their capability for detecting, classifying, and locating faults in PV systems [17]. In the literature, different types of artificial neural networks (ANN) have been applied for fault identification and diagnosis in PV systems. For example, a convolutional neural network-based approach is suggested for this purpose in [18]. Also, in [19], a two-stage support vector machine is used for fault detection in photovoltaic arrays. The merits of these methods are their high accuracy in detecting and locating different faults, fast decision making, and robustness against environmental noise. Although machine learning-based methods can be quite advantageous, they require large amounts of historical data for the training procedure. In general, the performance of a machine learning algorithm mainly depends on the quality of the training data it trains with. While gathering training data might be time-consuming and costly. Furthermore, these techniques have computational and implementational complexity, especially for outsized PV systems. On the other hand, the model is configured on a case-by-case basis. Consequently, it will be appropriate for supervising a particular PV system, but results may not be extensible to other PV systems.

To overcome the drawbacks of existing methods, further research is needed to put forward simple yet effective schemes for PV array protection. This paper proposes a comprehensive protection method to i) detect, ii) discriminate, and iii) locate electric faults in PV arrays. The main contributions of the proposed method are:

- Greater sensitivity that enables the detection of high impedance faults in PV arrays;
- Desirable reliability to discriminate electric faults from other mismatches, e.g., partial shading, independently of meteorological data;
- Locating faulty string with a minimal number of current and voltage sensors based on the concept of state variables.

The rest of this paper is organized as follows. Section II describes the PV system model. In Section III, the static and dynamic models of PV cells are detailed to formulate the behavior of PV cells during different conditions. Section IV puts forward the proposed method, which is evaluated using the PSCAD-EMTDC software in Section V. In Section VI, a comparison of the proposed scheme and other methods is provided. Finally, Section VII concludes the paper.

2. PV system model

Fig. 1 shows the schema of a grid-connected photovoltaic system with a central inverter structure, which is modeled in PSCAD-EMTDC. As shown in Fig. 2, the PV array is composed of M parallel strings, each of which consists of N series modules. The main specifications of the PV modules under standard test conditions (STC) [irradiance: 1000 W/m^2, temperature: 25℃, air mass: 1.5] are listed in Table 1 [20]. For each module, a bypass diode is implemented in reverse bias mode to decrease the effects of shading on the performance of the PV array. If the photocurrent of the shaded module falls below the output current of other PV modules, the bypass diode of the shaded module becomes forward biased to prevent the current reduction of non-shaded modules in the string. The maximum power point tracking (MPPT) based on the perturb and observe method is implemented to generate switching signals for the boost DC/DC converter to extract the maximum possible power [21]. A three-phase inverter is used to connect the PV system to the AC grid. Switching signals for the inverter are generated based on the control method presented in [22]. Finally, the transformer raises the output voltage of the inverter to the distribution grid's level. Although the modeled system has a central inverter structure, the proposed method can be applied to all other structures such as string inverter or module inverter structures. The central structure is selected because it involves all challenges of other structures and has additional problems, e.g., faulty string locating.

Based on Fig. 2, four types of electric faults (F1-F4) are possible in a PV array, namely ground fault, intra string line-to-line fault, cross string line-to-line fault, and open-circuit fault. According to National Electric Code (NEC) article 690, the PV module frames and other exposed non-current-carrying metal parts of the equipment should be grounded [23]. This is referred to as equipment grounding and is illustrated in Fig. 2 by green dashed lines. Ground fault (F1) is an unintentional connection between an energized conductor and earth/equipment grounding conductor [4]. As mentioned in [3], the ground fault is the most common fault among the electric failures of PV arrays. If a ground fault is not detected, it may lead to severe consequences, including dc arcs and fire hazards [3,4]. Therefore, NEC mandates ground fault protection for PV arrays. In the conventional protection scheme, the negative terminal of the PV array is connected to the ground through the

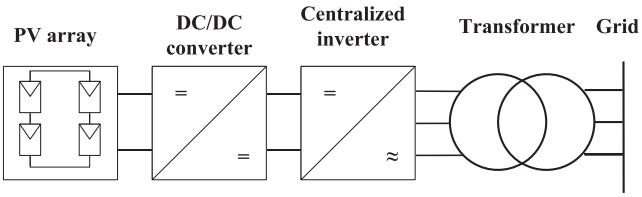

Fig. 1. Schematic diagram of a grid-connected photovoltaic system.

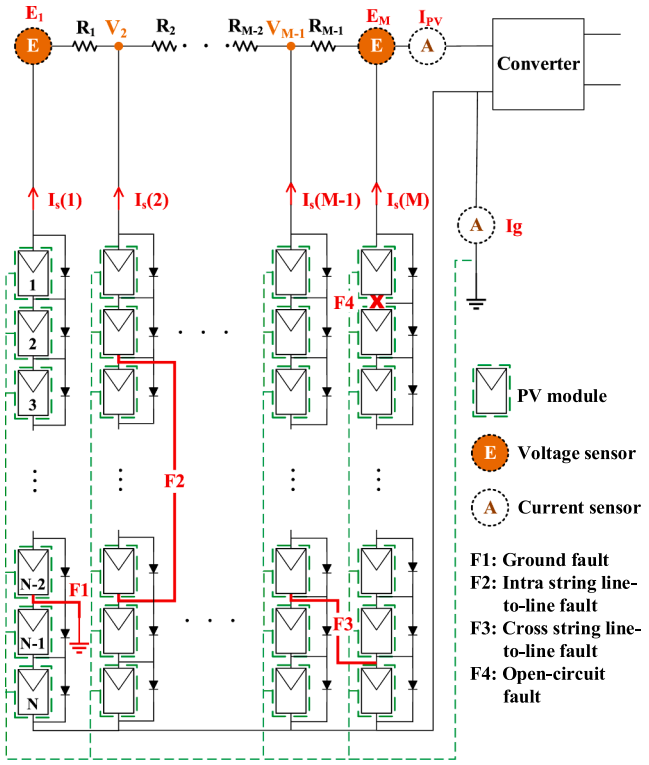

Fig. 2. PV array layout and types of electric faults.

Table 1
Characteristics of the PV Modules under STC.

PV module type	TBM72-375 M
Maximum power (P_{max})	375 (W)
Maximum power voltage (V_{mp})	39.79 (V)
Maximum power current (I_{mp})	9.43 (A)
Open-circuit voltage (V_{oc})	48.18 (V)
Short-circuit current (I_{sc})	9.91 (A)

Ground Fault Protection Device (GFPD). This practice is commonly referred to as system grounding [23]. Thanks to system grounding, the ground-fault current will always pass through the GFPD. When the fault current exceeds the threshold current, the GFPD fuse is blown, and the circulating path of the ground fault is interrupted. Then the inverter will be shut down, and the PV system will be isolated from the rest of the grid [4]. Based on UL 1741, the rating of the GFPD fuse ranges from 1 to 5 Ampere depending upon the size of.

converter. If a high impedance ground fault occurs at a location with a low potential to the ground, the fault current is lower than the rating of the GFPD, and the ground fault may go unnoticed. This gap is known as the blind spot of the conventional protection scheme. The following ground fault will result in a high fault current that blows out the GFPD fuse. However, the fault current will not be interrupted due to the presence of the first undetected fault [1,24]. This issue leads to substantial damages and ignites a fire in the PV system, as reported in Bakersfield, CA, USA, and Mount Holly, NC, USA [4,24]. In addition to the blind spot of existing protection practice, the performance of GFPD fuses can also be affected by low irradiance level, the response of MPPT to ground faults, non-linear PV characteristics, the presence of external noise, and leakage current [1,4].

Line-to-line fault is an accidental short circuit between two points in a PV array with different potentials. Line-to-line fault is divided into two types: 1) Intra string line-to-line fault (F2) and 2) Cross string line-to-line fault or string-to-string fault (F3). The severity of line-to-line faults is determined by the potential difference between two fault points, and the severe line-to-line fault might reverse the current flow through the faulty string [1]. Conventionally, line-to-line faults are detected and cleared by over-current protection devices (OCPD) that are connected in series with each string. The rating current of the OCPD fuse shall be at least 156% of the PV string's rated short-circuit current [23]. If the reverse fault current exceeds the threshold current, the OCPD fuse melts according to its time–current characteristics [4]. However, the magnitude of the fault current may be limited by high fault resistance, low solar irradiance, MPPT response, the presence of the blocking diode, and a low-mismatched fault location [1,3,4]. Consequently, fault detection will be more challenging, and the OCPDs may fail to detect these types of line-to-line faults in the PV arrays. And it results in a long-term degradation in power generation, as well as the risk of fire [4].

Although the existing protection practice is inexpensive and easy to implement, it does not guarantee reliable fault detection. Besides, there is no specific protection scheme for the open-circuit fault (F4). This fault occurs when one of the current-carrying paths in a PV array becomes disconnected [1]. Undetected open-circuit faults can generate series dc arcs and potentially cause a fire [2]. Hence, to address the shortcomings of the conventional fault detection approaches, this research proposes a new protection scheme to detect, discriminate, and locate discussed faults in PV arrays. In this regard, the static and dynamic models of PV cells are reviewed in the following section to formulate their behavior under the foregoing faults.

3. Static and dynamic model of the PV cell

Fig. 3 demonstrates an equivalent electric circuit that models a PV cell in a static sense. Accordingly, the output current of the PV cell can be calculated from the following equations [21]:

$$I = I_{ph} - I_d - I_{sh} \tag{1}$$

$$I_{ph} = I_{scn}(G/G_{ref})[1 + \alpha_T(T - T_{ref})](1 + R_s/R_{sh}) \tag{2}$$

$$I_d = I_0[exp(\frac{V + R_s I}{n(K_B T/q)}) - 1] \tag{3}$$

$$I_{sh} = (V + R_s I)/R_{sh} \tag{4}$$

By substituting (2)-(4) into (1), the output current characteristic versus the terminal voltage of the PV cell (I–V curve) is obtained. In normal conditions, the MPPT unit guarantees that the operating point on the I–V curve corresponds to the maximum power point (MPP) [21].

In abnormal conditions, the operating point of the PV cells moves away from MPP, and the static model is no longer valid [25]. Understanding the transient mode of the PV cells during short-circuit faults or the other transients requires the dynamic model of PV cells [25]-[27]. Fig. 4 shows the equivalent circuit for a PV cell's dynamic model as described in [27,28]. The dynamic equivalent circuit can be reduced to a single-time-.

constant resistance–capacitance circuit that has a first-order natural transient response [26,29]. Therefore, the PV cell's output current will be an exponential waveform when the voltage changes stepped. This condition occurs during short-circuit or open-circuit transient periods,

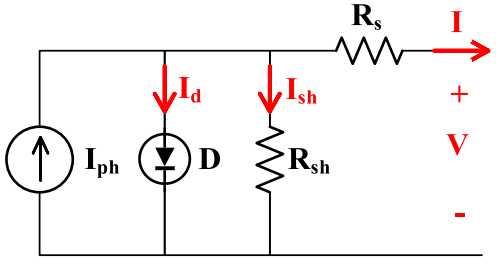

Fig. 3. Equivalent circuit of a photovoltaic cell in steady-state.

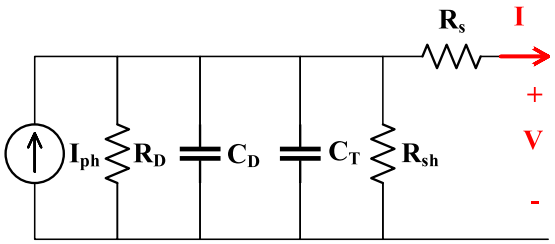

Fig. 4. Equivalent circuit of the PV cell's dynamic model.

as verified by simulation results. Following other disturbances, however, the output current would include different waveforms based on the dynamic model. For example, during the shading phase, photocurrent (I_{ph}) changes according to irradiation variations [26]. In this paper, the contrast between the output current's waveforms is utilized to differentiate electric faults from other disturbances.

4. Proposed method

The proposed method consists of the following stages: A) Disturbance detection, B) Discrimination of electric faults from other disturbances, and C) Faulty string location.

A. Disturbance Detection

To detect disturbance inception in the PV array, the following steps are taken:

Step 1: The difference between the PV array's output current from the corresponding average value is calculated from:

$$\Delta I_{PV} = \left| I_{PV} - I_{PV,\ avg} \right| \tag{5}$$

Step 2: ΔI_{PV} is compared with the threshold value of the PV array's current variations. If ΔI_{PV} is larger than a pre-determined threshold, say *ThD*, it can be concluded that the PV array is not operating in the normal mode.

Step 3: Larger values of ΔI_{PV} result from larger fault currents, which implies a more significant need for clearing the fault. To account for this, a cumulative deviation logic is developed. If the value of ΔI_{PV} exceeds ThD, it is added to G(k-1), which is the sum of the previous relative deviations. Otherwise, G(k-1) is halved (formulated in Fig. 5). The initial value of the counter (i.e., G(0)) is set to zero.

Step 4: If the value of the counter $G(k)$ exceeds a pre-determined threshold, denoted by *ThF*, it can be concluded that a disturbance has occurred in the PV array.

The values of *ThD* and *ThF* should be set as small as possible to increase the sensitivity of the detection method to high impedance faults whilst guarantying enough security against noise and other transient fluctuations. In this regard, various simulation studies should be conducted to test the suitability of these values in the various normal and abnormal conditions. Nevertheless, for the first assumption and typical value, 0.1% of the PV array output current is suitable for ThD, and the product of *ThD* and sampling frequency is a good approximation for ThF. The appropriate values selected for *ThD* and *ThF* in this paper are 0.01 and 100, respectively.

B. Discrimination

The static and dynamic models put forward in section III for a PV cell make it possible to differentiate electric faults from other disturbances. Based on the PV cell's dynamic model, the current signal during short-circuit and open-circuit faults involves an exponential component, making it different from the current signal following other disturbances. For example, in the partial shading mode, there is a linear relationship between the photocurrent (I_{ph}) and shading percentage.

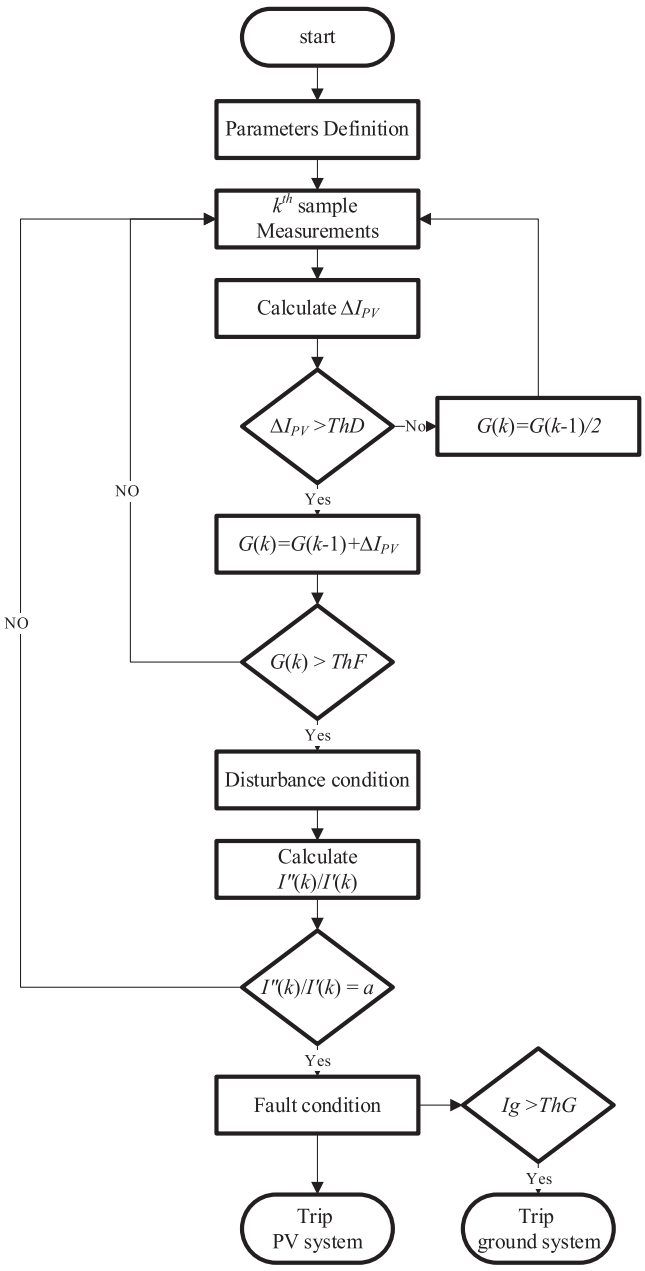

Fig. 5. Fault detection and discrimination flowchart.

Since the exponential function and its derivatives have similar waveforms, they differ only by constant ratios. This unique feature can be illustrated mathematically as below:

$$f(x) = exp(a.x)$$
$$\frac{f'(x)}{f(x)} = \frac{a.exp(a.x)}{exp(a.x)} = \frac{f''(x)}{f'(x)} = \frac{a^2.exp(a.x)}{a.exp(a.x)} = a \tag{6}$$

where a is the time constant of the exponential waveform, which is determined by the dynamic model. In this paper, the ratio of the second and first derivatives is used to identify the exponential waveform. After disturbance detection, if this ratio has the same value for several consecutive samples (10 samples in this paper), the electric fault is detected. And the protection system isolates the PV system from the grid. In order to calculate the first and second derivatives of the PV array current's k^{th} sample, the following equations, as described in [30], are used respectively:

$$I^{'}(k) = \frac{I_{PV}(k+1) - I_{PV}(k-1)}{2.\Delta T} \tag{7}$$

$$I''(k) = \frac{I_{PV}(k+1) - 2.I_{PV}(k) + I_{PV}(k-1)}{(\Delta T)^2} \tag{8}$$

where ΔT is the time interval between the two consecutive samples.

Based on Fig. 2, the ground fault current closes its path through the Ig sensor, which is essentially used to differentiate ground faults from other failures. If the current passing through the Ig sensor exceeds *ThG*, it can be concluded that a ground fault has occurred. Although the value of *ThG* should be as low as possible, the minimum value for *ThG* is determined based on the maximum value of the PV modules leakage current. Reference [24] presents an estimation method for the leakage current and concludes that the maximum value of the leakage current is 11 μA/kW. Therefore, $ThG = 0.01$ A will be an appropriate threshold for the simulated PV system. Although a large safety margin has been applied by choosing this threshold, it still offers much more sensitivity compared to the existing methods such as GFPD. Furthermore, the proposed method in this paper is more secure than the GFPD fuse because it utilizes another procedure for fault detection and uses the ground path current just for fault type classification. It should be noted that the proposed method cannot classify other types of electric faults (i.e., intra string line-to-line fault, cross string line-to-line fault (string to string fault), and open-circuit fault). For this purpose, more measurements are needed, or other methods should be conducted.

The flowchart of detection and discrimination steps is illustrated in Fig. 5. According to this figure, the proposed algorithm is very straightforward and could be applied to all structures such as central inverter, string inverter, module inverter. In addition to fault detection and discrimination, faulty string location is a crucial challenge for big solar farms which uses central inverter structure. In this regard, in the following part, the location procedure is perused.

C. Faulty-String Location

In order to detect fault occurrence in any string using the proposed method, it is needed to measure the current of each string by an individual sensor. In this section, the number of measurement sensors is minimized by using the concept of state variables. To adopt this concept, the state variables of the photovoltaic array should be specified. At the first step, it is assumed that the current variations of the healthy strings are negligible during the fault condition, i.e., healthy strings continue to generate the same amount of current as the pre-fault current. The reason for this assumption is that neither irradiation nor temperature significantly changes over the fault period. In addition, due to the non-linear characteristic of the current–voltage (I–V) curve, the current variations because of the PV array's voltage decline remain very small over the fault period. In this condition, the current variations of the healthy and faulty strings can be expressed as below:

$$\begin{cases} \Delta I_s(i) \approx 0 & i \neq i_F \\ \Delta I_s(i_F) \approx I_{fault} - I_{pre-fault} & i = i_F \end{cases} \tag{9}$$

where $\Delta I_s(i)$ is the current change in an arbitrary healthy string, i_F represents the faulty string, and $\Delta I_s(i_F)$ is the current change in the faulty string. Also, I_{fault} indicates the current that flows through the faulty string over the fault period, and $I_{pre\text{-}fault}$ denotes the current of the strings prior to the fault.

In the next step, the voltage variations of the strings are calculated. According to Fig. 2, the voltage change of the last string (ΔV_M) is measured by the voltage sensor E_M. Based on KVL and KCL, the voltage change of the string $M-1$ ($\Delta V_{M\text{-}1}$) is obtained to be:

$$\Delta V_{M-1} = \Delta V_M + R_{M-1}\left(\sum_{j=1}^{M-1} \Delta I_s(j)\right) \tag{10}$$

Furthermore, the voltage change of an arbitrary string (i^{th} string) can be calculated based on the voltage variation of the next string as:

$$\Delta V_i = \Delta V_{i+1} + R_i\left(\sum_{j=1}^{i} \Delta I_s(j)\right) \tag{11}$$

Similarly, the voltage variation of the string $i+1$ can be written based on the voltage change of the string $i+2$, and it can.

be combined with (11) as follows:

$$\Delta V_i = \Delta V_{i+2} + R_{i+1}\left(\sum_{j=1}^{i+1} \Delta I_s(j)\right) + R_i\left(\sum_{j=1}^{i} \Delta I_s(j)\right) \tag{12}$$

Using the induction principle, the voltage variation of the i^{th} string can be obtained in terms of the voltage change of the last string (ΔV_M), resistances between i^{th} string and the last string, and current variations of the strings as follow:

$$\begin{aligned} \Delta V_i = \Delta V_M + R_{M-1}\left(\sum_{j=1}^{M-1} \Delta I_s(j)\right) + R_{M-2}\left(\sum_{j=1}^{M-2} \Delta I_s(j)\right) \\ + \cdots + R_{i+1}\left(\sum_{j=1}^{i+1} \Delta I_s(j)\right) + R_i\left(\sum_{j=1}^{i} \Delta I_s(j)\right) \end{aligned} \tag{13}$$

Based on (9), the sum of the current variations of the strings to the left of the faulty string is zero, but the sum of the current variations of the strings to the right of the faulty string is equal to the current variation of the faulty string. This can be mathematically expressed as below:

$$\begin{aligned} &\sum_{j=1}^{p} \Delta I_s(j) = 0, \qquad p = 1, \cdots, i_F - 1 \\ &\sum_{j=1}^{i_F} \Delta I_s(j) = \sum_{j=1}^{i_F+1} \Delta I_s(j) = \cdots = \sum_{j=1}^{M} \Delta I_s(j) = \Delta I_s(i_F) \end{aligned} \tag{14}$$

By combining (13) and (14), the voltage variations in the strings to the right of the faulty string are obtained to be.

$$\Delta V_i = \Delta V_M + \left(\sum_{j=i}^{M-1} R_j\right)\Delta I_s(i_F) \qquad i \geqslant i_F \tag{15}$$

Based on (14), the sum of the current variations passing through the strings and lines to the left of the faulty string is equal to zero. In this regard, the voltage changes in the strings to the left of the faulty string are equal to the voltage change in the faulty string. Hence,

$$\Delta V_i = \Delta V_{i_F} = \Delta V_M + \left(\sum_{j=i_F}^{M-1} R_j\right)\Delta I_s(i_F) \quad i < i_F \tag{16}$$

According to (14), (15), and (16), variations of the strings' currents and voltages are dependent on three parameters: Last string voltage variation (ΔV_M), the current variation of the faulty string ($\Delta I_s(i_F)$), and the faulty string location. In other words, these three parameters are state variables of the PV system. Therefore, measurement sensors should be located in places where these state variables can be determined with the least number of sensors. In this regard, to determine ΔV_M, it is necessary to use the voltage sensor E_M, as shown in Fig 0.2. Furthermore, according to (9), the current variations of the healthy strings are negligible and can be assumed to be zero. Thus, the current change of the faulty string ($\Delta I_s(i_F)$) would be equal to the variation of the PV array's output current (ΔI_{PV}), which is measured by the current sensor I_{PV}. In order to determine the location of the faulty string, (15) can be rewritten to calculate the sum of the line resistances between the faulty string to the last string as follows:

$$\left(\sum_{j=i_F}^{M-1} R_j\right) = \frac{\Delta V_{i_F} - \Delta V_M}{\Delta I_s(i_F)} = \frac{\Delta V_{i_F} - \Delta V_M}{\Delta I_{PV}} \tag{17}$$

Based on (16), the voltage changes in the strings to the left of the faulty string are equal to the voltage change in the faulty string. Therefore, in all cases, the amount of the voltage variation in the faulty

string (ΔV_{iF}) is equal to the voltage change of the first string (ΔV_1), which is measured by the voltage sensor E_1. Therefore, (17) can be rewritten as follows:

$$(\sum_{j=i_F}^{M-1} R_j) = \frac{(\Delta V_1 - \Delta V_M)}{\Delta I_{PV}} \tag{18}$$

Now the sum of the line resistances between the faulty string and the last string is calculated. By knowing the value of the line resistance between consecutive strings, the location of the faulty string can be easily estimated. In a special case, if the resistance among consecutive strings is identical (and is equal to R_{str}), the location of the faulty string (FL) can be obtained from:

$$(\sum_{j=i_F}^{M-1} R_j) = (M - FL)R_{str} = \frac{(\Delta V_1 - \Delta V_M)}{\Delta I_{PV}} \tag{19}$$

$$FL = round(M - \frac{\Delta V_1 - \Delta V_M}{\Delta I_{PV}.R_{str}}) \tag{20}$$

The round function is applied in (20) to account for measurement errors and parameter inaccuracies. It should be noted that similar to ΔI_{PV}, the differences between the first/last string voltage from the corresponding average values are employed as $\Delta V_1/\Delta V_M$ in the above equations. Despite the inaccuracies and approximations, the results of faulty string location are very acceptable, as shown in the next section. As can be seen from (18) and (20), only the measurement of i) voltage of the first string, ii) voltage of the last string, and iii) the output current of the PV array will be enough for fault location. And this is independent of the number of parallel strings in a solar power plant.

5. Performance evaluation

To evaluate the performance of the proposed method, a 37.5-kW photovoltaic array including 10 parallel strings, each one consisting of 10 series modules, is simulated using PSCAD-EMTDC. All measured signals are sampled at a 10-kHz frequency. To attenuate the noise effect, a first-order low-pass Butterworth filter with the cut-off frequency f_c = 50 Hz is adopted. It should be noted the simulation cases are conducted in the presence of white Gaussian noise with SNR = 80 dB. Based on the output results, the proposed scheme is secure against noise. MATLAB is used to implement the proposed method.

A. High Impedance Ground Fault

Fig. 6 demonstrates the variations of the PV array's output current, the ground system's current, and the voltages of the first and last strings when a ground fault has occurred in the last module of the 5th string with R_F = 50 Ω fault resistance. Although the current and voltage variations are very small, the proposed method detects the disturbance 36.5 ms after the fault inception. Fig. 7 shows the first and second derivatives curves of the PV array's output current. According to Fig. 7, both curves have exponential waveforms during the fault period, similar to the PV array output current. Therefore, the fault condition is detected, and the PV system is isolated from the grid. As can be seen from Fig. 6 (b), the current passing through the Ig sensor is equal to 0.7 A, which exceeds the ThG threshold. Therefore, the fault type is correctly identified to be the ground fault. Based on (20) and using the measured values ΔI_{PV} = –0.19 A, ΔV_1 = –0.06 V, and ΔV_{10} = –0.05 V, extracted from Fig. 6(a), 6(c), and 6(d), respectively, faulty string is obtained to be the 5th string, assuming R_{str} = 0.01 Ω. It is worth noting that, since the ground path current (Ig = 0.7 A) is less than the minimum rating of GFPD (i.e., 1 A), this fault is not be detected by conventional protection practice and thus remains in the PV system as a blind spot. However, the proposed method identifies the occurrence and location of the fault accurately and avoids the prospective risks.

Table 2 summarizes the proposed method's performance for ground

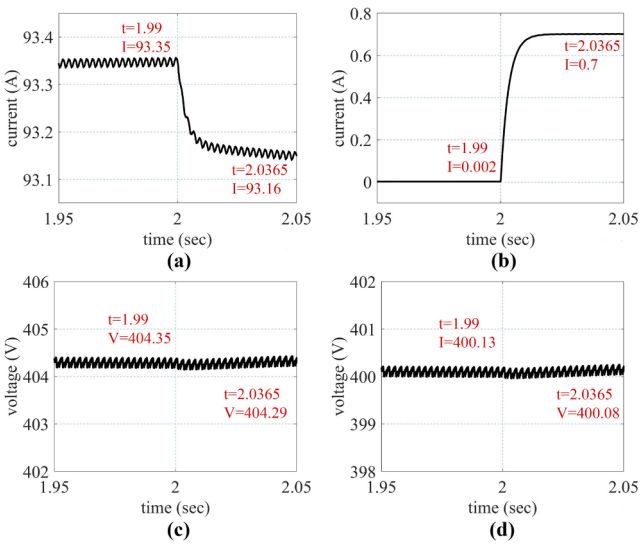

Fig. 6. a) PV array output current, b) Ground system current, c) First string voltage, d) Last string voltage variations in the case of the ground fault in 5th string.

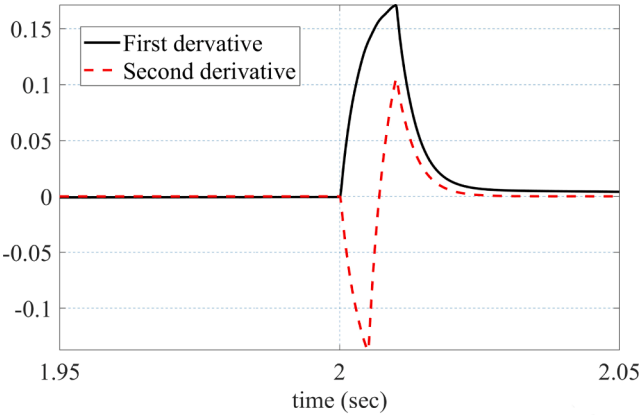

Fig. 7. The curve of the first and second derivatives of the PV array current during the ground fault.

Table 2
Performance of the Proposed Method for Ground Fault.

Studied Cases		(1)	(2)	(3)	(4)	(5)
Faulty String	Real	5	1	4	7	9
	Diagnosed	5	1	4	7	10
Faulty module		10	5	6	2	8
Fault resistance (Ω)		20	20	20	20	20
Detection time (ms)		12.6	4.7	5.1	4.3	6.2
Studied Cases		(6)	(7)	(8)	(9)	(10)
Faulty String	Real	5	5	5	5	5
	Diagnosed	5	5	5	5	5
Faulty module		10	10	10	10	10
Fault resistance (Ω)		0	20	50	75	100
Detection time (ms)		5	12.6	36.5	73.1	117.9

faults in various locations with a range of fault resistances. Based on Table 2, the increase in the magnitude of the fault resistance decreases the fault detection speed. However, excluding high impedance faults, it can be confirmed that the proposed method can detect the fault occurrence in the PV array within a few milliseconds following the disturbance inception. Furthermore, the location of the faulty string has been pinpointed with great precision.

B. Effect of Partial Shadow

In this section, the security of the proposed method is investigated against the partial shading mode. To do this, the irradiation of a single module in the last string is reduced from 1000 W/m2 to 200 W/m2 within 100 ms. Therefore, the array output current decreases, as shown in Fig. 8(a). It is worthful to note that the bypass diode is activated for the shaded module in this case. The disturbance occurrence has been detected in 15.4 ms after the beginning of the shadow. Based on (20) and using the measured values $\Delta I_{PV} = -0.39$ A, $\Delta V_1 = -0.39$ V, and $\Delta V_{10} = -0.35$ V, from Fig. 8(a), 8(c), and 8(d), respectively, it can be deduced that the last string is disturbed, assuming $R_{str} = 0.01\ \Omega$.

As shown in Fig. 9, neither the first nor the second derivative of the PV output current has an exponential waveform during the shadow period. This is why no short-circuit fault is identified, and the protection system does not issue a trip command.

Table 3 shows the performance of the proposed method for partial shading in the different conditions. Obtained results confirm that the method can successfully detect the disturbance inception and reliably differentiate it from short-circuit faults.

C. Simultaneous Faults

In this section, the performance of the proposed method is assessed against simultaneous faults. To do so, it is assumed that a partial shading occurs in the last string at $t_1 = 3$ sec, similar to the previous case. Therefore, the current and voltage variations are equal to those in case *B*, and the protection system acts in the same way. At t = 4 sec, a line-to-line fault occurs within the same string simultaneously. In this fault, the terminals of a single PV module are externally short-circuited without fault resistance $R_F = 0\ \Omega$. The variations of the PV array output current, ground system current, and voltages of the first and last strings are shown in Fig. 10. The proposed method detects the disturbance 8.6 ms following the fault inception. As shown in Fig. 11, the first and second derivates of the PV array's current have exponential waveforms over the fault period. Hence, the fault condition is discriminated from the previous shading mode, and the PV system should be isolated from the grid. It is noted that $\Delta I_{PV} = -3.4$ A, $\Delta V_1 = -3.42$ V, $\Delta V_{10} = -3.09$ V, from Fig. 10(a), 10(c), and 10(d), respectively. Using (20) and assuming $R_{str} = 0.01\ \Omega$, the 10th string is identified as being faulty. As mentioned before, the proposed method can not identify the type of fault in the case

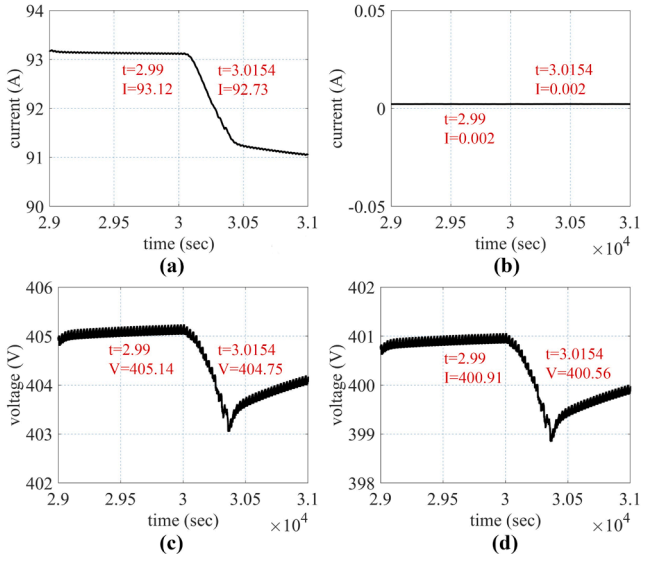

Fig. 8. a) PV array output current, b) Ground system current, c) First string voltage, d) Last string voltage variations in the case of partial shading in the last string.

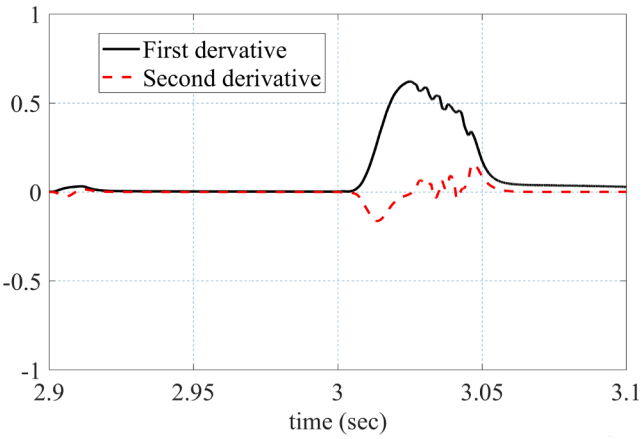

Fig. 9. The curve of the first and second derivatives of the PV array current during partial shading.

Table 3
Performance of the Proposed Algorithm for Partial Shadow.

Studied case		(1)	(2)	(3)	(4)
Shaded string	Real	10	1	1	1
	Diagnosed	10	1	1	1
Irradiance (W/m^2)	Pre shadow	1000	1000	1000	800
	During shadow	200	200	200	400
Shading time (ms)		100	100	50	100
Number of shaded modules		2	1	1	1
Detection time (ms)		14.5	16.5	10.9	37.7
Fault occurrence detection		NO	NO	NO	NO

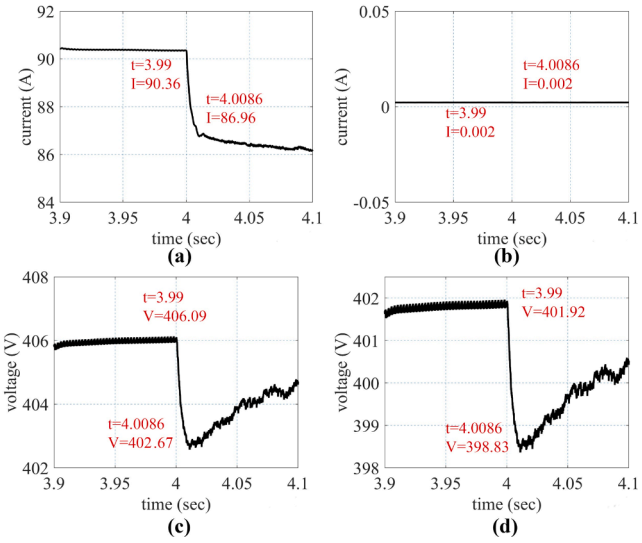

Fig. 10. a) PV array output current, b) Ground system current, c) First string voltage, d) Last string voltage variations in the case of simultaneous line-to-line fault.

of line-to-line or open-circuit faults. This case is a protection gap of conventional protection devices. Because of initial shading, the current value of the last string is small. In addition, the fault location mismatch is minimal, and only one module is faulted. Thus, the current passing through the OCPD fuse is about 2 A, far less than its rating (i.e.,$1.56 \times 9.91 = 15$ A). As a result, the fault remains uncleared in the PV array and decreases the output power of the solar power plant. On the other hand, the proposed approach could detect the occurrence and location of the fault in just 8.6 ms following the fault inception.

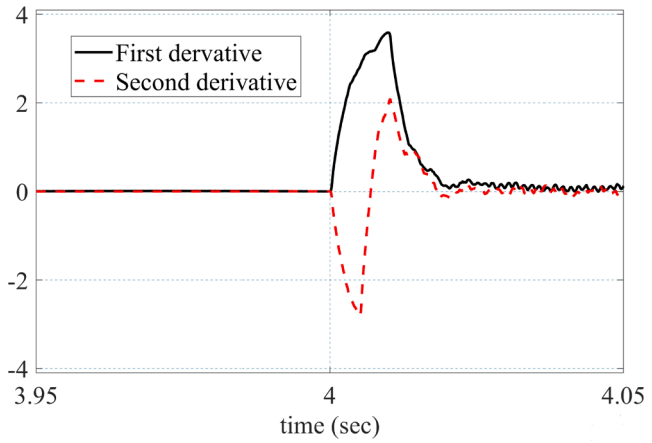

Fig. 11. The curve of the First and second derivatives of the PV array current during the simultaneous line-to-line fault.

Table 4 shows the performance of the proposed method in some cases of simultaneous faults. Where (SH) refers to partial shadow, (GF) refers to the ground fault, and (LL) refers to the line-to-line fault. The obtained results show that the method can detect simultaneous faults irrespective of the previous state, thanks to its sensitivity to current and voltage variations.

6. Comparison

The structure of signal processing-based methods is different from the proposed method. Besides, each data driven-based method has particular and own-developed datasets and model configurations. Therefore, the comparison of methods with the different categories is pretty difficult. In this regard, Table 5 compares the proposed method in this paper and state-of-the-art techniques, which fall in the quantitative model-based category.

Where M is the number of parallel strings in a PV array. According to Table 5, although some approaches take less time to detect the fault, they require a massive number of measurement sensors. For example, if a PV array has M = 10 parallel strings, the conventional protection system requires 11 fuses, and methods suggested in [6,7], and [8] need 12, 21, and 22 voltage and current sensors, respectively. However, the proposed method in this paper requires just 4 measurement sensors. Therefore, the Implementation of the proposed method for large-scale PV powerplants will be very affordable.

7. Conclusion

In this paper, a novel protection scheme is proposed to detect, discriminate, and locate various types of electric faults in the PV arrays. Simulation results confirm that the proposed method has superior sensitivity in detecting high-impedance faults. A new technique is introduced based on the waveform of the PV array current to discriminate electric faults from other disturbances with great reliability. Although the increment in the fault resistance does not have a significant impact on the fault discrimination and location procedures, it does decelerate the fault detection speed slightly. The foregoing features are verified by simulating a prototype solar power plant using PSCAD-EMTDC. The need for a minimal number of measurements is the salient advantage of the proposed method over existing ones. Adopting the state variables concept provides this salient feature that measuring the PV array's output current, ground's path current, and the voltages of the first and the last string will be sufficient to protect the entire strings of a PV array. The proposed method will be an attractive solution for practical applications as its implementation cost is minimal without endangering the security and dependability of the protection system.

Table 4
Performance of the Proposed Method in Simultaneous Faults.

Studied case		(1)	(2)	(3)	(4)
First faulty string	Real	10	1	5	8
	Diagnosed	10	1	5	9
First fault type		SH	SH	LL	GF
Fault resistance (Ω)		–	–	0	20
Detection time (ms)		15.4	18.0	5.0	4.3
Second faulty string	Real	1	9	3	2
	Diagnosed	1	9	3	1
Second fault type		LL	GF	GF	GF
Fault resistance (Ω)		0	20	0	0
Detection time (ms)		8.5	7.8	5.0	5.1

Table 5
Comparison of the proposed method and other methods.

Method	Existing practice	[6]	[7]	[8]	Proposed method
Fault diagnosis from partial shading	–	Yes	Yes	Yes	Yes
Independence from meteorological data	No	Yes	Yes	Yes	Yes
Detection time (ms)	–	200	1–15	0.1–0.4	4–120
Detection of high impedance faults	No	No	Yes	Yes	Yes
Fault locating	No	Yes	Yes	No	Yes
Number of required measurements	M + 1	M + 2	2 M + 1	2 M + 2	4

CRediT authorship contribution statement

Hossein Bagherzadeh: Conceptualization, Investigation, Software, Writing – original draft. **Moein Abedini:** Supervision, Writing – review & editing. **Mahdi Davarpanah:** Supervision, Writing – review & editing. **Sadegh Azizi:** Writing – review & editing.

Declaration of Competing Interest

The authors declare that they have no known competing financial interests or personal relationships that could have appeared to influence the work reported in this paper.

References

[1] Pillai DS, Rajasekar N. A comprehensive review on protection challenges and fault diagnosis in PV systems. Renew Sustain Energy Rev Aug. 2018;91:18–40.
[2] Yuventi J. DC electric arc-flash hazard-risk evaluations for photovoltaic systems. IEEE Trans Power Delivery Feb. 2014;29(1):161–7.
[3] Mellit A, Tina GM, Kalogirou SA. Fault detection and diagnosis methods for photovoltaic systems: A review. Renew Sustain Energy Rev Aug. 2018;91:1–17.
[4] Alam MK, Khan F, Johnson J, Flicker J. A Comprehensive Review of Catastrophic Faults in PV Arrays: Types, Detection, and Mitigation Techniques. IEEE J Photovoltaics May 2015;5(3):982–97.
[5] S. Sarikh, M. Raoufi, A. Bennouna, A. Benlarabi, and B. Ikken, "Fault diagnosis in a photovoltaic system through I-V characteristics analysis," *2018 9th International Renewable Energy Congress (IREC)*, Hammamet, Tunisia, 2018, pp. 1-6.
[6] Ch. Li, Y. Yang, K. Zhang, Ch. Zhu, and H. Wei, "A fast MPPT-based anomaly detection and accurate fault diagnosis technique for PV arrays," in *Energy Conversion and Management,* vol. 234, p. 113950, Apr. 2021.
[7] Saleh KA, Hooshyar A, El-Saadany EF, Zeineldin HH. Voltage-Based Protection Scheme for Faults Within Utility-Scale Photovoltaic Arrays. IEEE Trans Smart Grid Sept. 2018;9(5):4367–82.
[8] H. A. Abd el-Ghany, A. E. ELGebaly, and I. B. M. Taha, "A new monitoring technique for fault detection and classification in PV systems based on rate of change of voltage-current trajectory," in *International Journal of Electrical Power & Energy Systems,* vol. 133, p. 107248, Dec. 2021.
[9] Chouder A, Silvestre S. Automatic supervision and fault detection of PV systems based on power losses analysis. Energy Convers Manage Oct. 2010;51(10):1929–37.
[10] Yao X, Herrera L, Ji S, Zou K, Wang J. Characteristic Study and Time-Domain Discrete- Wavelet-Transform Based Hybrid Detection of Series DC Arc Faults. IEEE Trans Power Electron June 2014;29(6):3103–15.

[11] Kumar BP, Ilango GS, Reddy MJB, Chilakapati N. Online Fault Detection and Diagnosis in Photovoltaic Systems Using Wavelet Packets. IEEE J Photovoltaics Jan. 2018;8(1):257–65.
[12] M. Murtadho, E. Prasetyono, and D. O. Anggriawan, "Detection of Parallel Arc Fault on Photovoltaic System Based on Fast Fourier Transform," *2020 International Electronics Symposium (IES)*, Surabaya, Indonesia, 2020, pp. 21-25.
[13] L. Schirone, F. P. Califano, U. Moschella, and U. Rocca, "Fault finding in a 1 MW photovoltaic plant by reflectometry," *Proceedings of 1994 IEEE 1st World Conference on Photovoltaic Energy Conversion - WCPEC (A Joint Conference of PVSC, PVSEC, and PSEC)*, Waikoloa, HI, USA, 1994, pp. 846-849, vol. 1.
[14] T. Takashima, J. Yamaguchi, and M. Ishida, "Fault detection by signal response in PV module strings," *2008 33rd IEEE Photovoltaic Specialists Conference*, San Diego, CA, USA, 2008, pp. 1-5.
[15] Vergura S, Acciani G, Amoruso V, Patrono GE, Vacca F. Descriptive and Inferential Statistics for Supervising and Monitoring the Operation of PV Plants. IEEE Trans Ind Electron Nov. 2009;56(11):4456–64.
[16] Y. Zhao, B. Lehman, R. Ball, J. Mosesian, and J. d. Palma, "Outlier detection rules for fault detection in solar photovoltaic arrays," *2013 Twenty-Eighth Annual IEEE Applied Power Electronics Conference and Exposition (APEC)*, Long Beach, CA, USA, 2013, pp. 2913-2920.
[17] B. Li, C. Delpha, A. Migan-Dubois, and D. Diallo, "Fault diagnosis of photovoltaic panels using full I–V characteristics and machine learning techniques," in *Energy Conversion and Management,* vol. 248, p. 114785, Nov. 2021.
[18] Aziz F, Ul Haq A, Ahmad S, Mahmoud Y, Jalal M, Ali U. A Novel Convolutional Neural Network-Based Approach for Fault Classification in Photovoltaic Arrays. IEEE Access 2020;8:41889–904.
[19] Yi Z, Etemadi AH. Line-to-Line Fault Detection for Photovoltaic Arrays Based on Multiresolution Signal Decomposition and Two-Stage Support Vector Machine. IEEE Trans Ind Electron Nov. 2017;64(11):8546–56.
[20] "TBM-72-365~375M PV Module Product Datasheet V4_EN," Taban Energy Dev. Co., Feb. 2019.
[21] S. Arno, J. Klaus, I. Olindo, V. S. Rene, and Z. Miro, *Solar Energy; The physics and Engineering of Photovoltaic Conversion, Technologies, and Systems*, Cambridge, England: UIT Cambridge Ltd, 2016.
[22] Pogaku N, Prodanovic M, Green TC. Modeling, Analysis, and Testing of Autonomous Operation of an Inverter-Based Microgrid. IEEE Trans Power Electron Mar. 2007;22(2):613–25.
[23] National Electrical Code, "Article 690-Solar Photovoltaic (PV) Systems," NFPA 70, 2014.
[24] G. Ball, B. Brooks, J. Johnson, J. Flicker, A. Rosenthal, J. Wiles, L. Sherwood, M. Albers, and T. Zgonena, "Inverter ground-fault detection 'blind spot' and mitigation methods," Solar America Board for Codes and Standard Report, Jun. 2013.
[25] Kim KA, Xu C, Jin L, Krein PT. A Dynamic Photovoltaic Model Incorporating Capacitive and Reverse-Bias Characteristics. IEEE J Photovoltaics Oct. 2013;3(4):1334–41.
[26] L. Qin, S. Xie, C. Yang, and J. Cao, "Dynamic model and dynamic characteristics of solar cell," *2013 IEEE ECCE Asia Downunder*, Melbourne, VIC, Australia, 2013, pp. 659–663.
[27] J. Johnson, D. Schoenwald, S. Kuszmaul, J. Strauch, and W. Bower, "Creating dynamic equivalent PV circuit models with impedance spectroscopy for arc fault modeling," *2011 37th IEEE Photovoltaic Specialists Conference*, Seattle, WA, USA, 2011, pp. 002328-002333.
[28] Chenvidhya D, Kirtikara K, Jivacate C. PV module dynamic impedance and its voltage and frequency dependencies. Sol Energy Mater Sol Cells Mar. 2005;86(2):243–51.
[29] Benavides ND, Chapman PL. Modeling the effect of voltage ripple on the power output of photovoltaic modules. IEEE Trans Ind Electron July 2008;55(7):2638–43.
[30] G. B. Gilcrest, G. D. Rockefeller, and E. A. Udren, "High-Speed Distance Relaying Using a Digital Computer I - System Description," in *IEEE Transactions on Power Apparatus and Systems*, vol. PAS-91, no. 3, pp. 1235-1243, May 1972.